Iranian Journal of Basic Medical Sciences
ijbms.mums.ac.ir

Repurposing an antimicrobial arginine-rich decapeptide as a novel anticancer agent: Evidence from *in vitro* and *in vivo* breast cancer models

Reyhane Chamani [1] *, Maryam Mohammadi [1]

[1] Department of Biology, Yazd University, Yazd, Iran

ARTICLE INFO

Article type:
Original

Article history:
Received: Oct 25, 2025
Accepted: Feb 22, 2026

Keywords:
Antineoplastic agents
Apoptosis
Cell cycle/drug effects
Dual-function peptide
Peptides/chemistry

ABSTRACT

Objective(s): Arginine-rich peptides have attracted interest because of their ability to interact with negatively charged cancer cell membranes. The present study aimed to evaluate the anticancer properties of a novel antimicrobial arginine-rich decapeptide (RL10) *in vitro* and *in vivo*.

Materials and Methods: Cytotoxicity was assessed in breast (4T1), colon (SW480), and normal fibroblast (NIH3T3) cell lines by MTT assay following 48- and 72-hr treatment (6-400 µg/ml). Membrane integrity was examined in 4T1 cells after 48 hr using lactate dehydrogenase (LDH) release. Flow cytometry was applied to determine apoptosis induction and alterations in cell cycle distribution. Caspase 3/7 activity was also evaluated. Apoptosis-related gene expressions were analyzed using RT-PCR. The antitumor effect of RL10 was assessed in a murine 4T1 model, followed by histopathological analysis using H&E staining.

Results: RL10 significantly declined cancer cell viability in a dose-dependent manner, with no toxicity on normal cells. No increase in LDH release was detected. Flow cytometry revealed 28.9% apoptosis induction and cell cycle arrest at the S and G2/M phases. Marked upregulation of the *Casp9* gene suggested possible activation of the intrinsic apoptotic pathway; however, *Bax*, *Bcl2*, *p53*, and *Casp8* expressions remained unchanged. *In vivo*, two weeks' treatment with the peptide suppressed tumor growth by nearly 39% ($P<0.01$), accompanied by increased apoptotic figures and reduced mitotic counts.

Conclusion: These findings provide the first evidence that an arginine-rich short peptide exhibits anticancer activity through apoptosis induction and tumor growth inhibition, underscoring its potential as a candidate for cancer therapy or drug delivery systems.

▶ Please cite this article as:
Chamani R, Mohammadi M. Repurposing an antimicrobial arginine-rich decapeptide as a novel anticancer agent: Evidence from *in vitro* and *in vivo* breast cancer models. Iran J Basic Med Sci 2026; 29: 736-743. doi: https://dx.doi.org/10.22038/ijbms.2026.92237.19905

Introduction

Cancer is one of the most important causes of mortality worldwide, and breast cancer represents a significant global health challenge. According to the World Health Organization (WHO), there were an estimated 2.26 million women diagnosed with breast cancer and 685000 deaths globally in 2020 (1). Search for novel therapeutic strategies that are both effective and safe continues to be a priority in biomedical research. In recent years, Anti-cancer peptides (ACPs) have gained increasing attention. They help develop new approaches that surpass the limitations of traditional therapy (2). Due to their high specificity, reduced side effects, and lower toxicity, these peptides have become a major therapeutic strategy for cancer treatment (3).

ACPs are typically amphipathic, positively charged, and possess natural antimicrobial properties, and can be used alone or in combination with immunotherapy and chemotherapy (4). Moreover, these peptides can be formulated with nanocarriers to enhance delivery and reduce degradation by the body's enzymes. Their anticancer properties include apoptosis induction, membrane disruption, angiogenesis inhibition, signaling pathway modulation, immunomodulation, and DNA damage (3, 5, 6).

Cationic arginine-rich peptides (CARPs) can be classified as anti-cancer peptides, which also have inherent neuroprotective, antimicrobial, and cardioprotective properties. CARPs possess a positive charge due to the presence of arginine and lysine residues. The membrane-penetrating ability of CARPs makes them promising candidates for therapeutic applications (7).

Despite the large number of cationic anticancer peptides studied to date, most remain constrained by key limitations, including low bioavailability and stability in biological environments, relative toxicity to normal cells, and limited clinical translation. Furthermore, subtle changes in peptide sequences can dramatically alter their selectivity, membrane penetration, and mechanisms of inducing cell death. Therefore, the discovery and characterization of novel cationic peptides remain highly valuable (8).

Certain properties of peptides overlap, such as the shared properties of ACPs and antimicrobial peptides

***Corresponding author:** Reyhane Chamani. Daneshgah Blvd, Department of Biology, Yazd University, Yazd, Iran. Tel: +98-35-31232652, Fax: +98-35-38210644, Email: chamani@yazd.ac.ir

(AMPs). Antimicrobial peptides are small peptides that play an important role in immune system mechanisms. They possess various therapeutic properties, including antibacterial, antiviral, antitumoral, immunomodulatory, and biofilm-inhibition activities (9). AMPs are usually cationic, amphipathic compounds with hydrophobically enriched residues. Consequently, they quickly interact with negatively charged microbial membranes, leading to microbial death. AMPs are low-mass, highly soluble, thermally stable, and low-cytotoxic molecules, making them promising antimicrobial agents (9). A wide range of cancer cells can be inhibited by AMPs. Cancer cells are structurally and chemically different from normal cells. Their underdeveloped cytoskeleton, abnormal presence of acidic phospholipids, and high metabolic rate make them more susceptible to AMPs than normal cells.

So, AMPs can easily penetrate their lipid membranes and destroy the cancer cells by forming ion channels, leading to cellular leakage (10, 11). Agrillo *et al.* characterized the antimicrobial activity of an arginine-rich decapeptide using the standard broth microdilution method against various bacteria, including *Listeria monocytogenes, Escherichia coli, Staphylococcus aureus, Salmonella Typhimurium,* and *Pseudomonas aeruginosa* (12). To date, its anticancer potential has not been investigated. Given its structural features, high cationic charge, and propensity to adopt amphipathic conformations, this peptide represents a promising candidate for evaluation in cancer models. Therefore, the present study aimed to investigate, for the first time, the anticancer properties of the peptide (Named RL10) *in vitro* and *in vivo*. Specifically, we assessed its cytotoxicity, ability to stimulate apoptosis and cell cycle arrest, effects on apoptosis-related gene expression, and tumor growth suppression in a murine breast cancer model. These findings provide novel insight into the therapeutic potential of short arginine-rich antimicrobial peptides as anticancer agents.

Materials and Methods

Materials

Dulbecco´s Modified Eagle Medium (DMEM), trypsin, Fetal Bovine Serum (FBS), and antibiotics were purchased from Gibco Invitrogen (Carlsbad, CA, USA). 3-(4,5-dimethylthiazol-2-yl)-2,5-diphenyltetrazolium bromide (MTT) and Dimethylsulfoxide (DMSO) were purchased from Sigma-Aldrich, USA. Trizol reagent was obtained from ELK Biotechnology, USA. Other chemicals and reagents were of analytical grade and purchased from Merck (Darmstadt, Germany). All the solutions were prepared in doubly distilled water. Other kits were as follows: Lactate dehydrogenase (LDH) colorimetric assay kit from Abcam, UK; Annexin V-FITC/PI apoptosis detection kit from Elabscience Bionovation Inc.; Caspase-3/7 colorimetric assay kit from Kiazist, Iran; cDNA synthesis kit from SinaClon BioScience, Iran; PCR Master Mix from Toyobo, Japan; Hematoxylin and Eosin (H&E) staining kit from AP-RAD, Iran.

Peptide synthesis

Shine Gene Bio-Company (China) synthesized the peptide with the sequence of $^{+}{}_{3}$HN-RLRWVRIWRR-COO^{-} (Named RL10). Its purity (~90%) and molecular weight (1496.83 Daltons) were explored by Mass spectrometry and HPLC, respectively (See supplementary file).

In vitro assays

Cell culture and MTT assay

4T1 (the murine mammary tumor cell line), SW480 (the human colorectal adenocarcinoma cell line), and NIH3T3 (the murine fibroblast cell line) were obtained from Pasteur Institute of Iran (Tehran, Iran) and cultured in DMEM with 20% FBS and incubated at 37 °C in 5% CO_2. Passages 4 were employed for the subsequent assays. 6.25, 12.5, 25, 50, 100, 200, and 400 µg/ml of the peptide were added to the wells containing 5×10^3 4T1 and SW480 cells and incubated for 48 and 72 hr. NIH3T3 cells were incubated for just 48 hr. After washing the treated cells with phosphate-buffered saline (PBS) and adding 5 mg/ml MTT to the wells, cells were incubated for 4 hr at 37 °C. Centrifugation was performed at 1000 x g for 5 min, and the medium was thrown away. The Formazan crystals were made soluble by 150 µl DMSO. The absorbance (A) at 570 nm was measured using a plate reader. Cell viability was calculated using the following formula and plotted as the average ± standard error (SE) of three tests (13).

$$\text{Cell viability \%} = [(A_{Treatment} - A_{Blank}) / (A_{Control} - A_{Blank})] \times 100$$

Dose-response curves were generated by plotting percentage of cell viability against the logarithm of peptide concentration, and IC_{50} values were calculated using nonlinear regression analysis.

Lactate dehydrogenase (LDH) release assay

LDH release was quantified using a commercial LDH colorimetric assay kit (Abcam, UK) according to the manufacturer's protocol. 4T1 cells were seeded in 96-well plates (8×10^3 cells per well) and treated with 67 µg/ml of the peptide for 48 hr. After incubation, culture supernatants (100 µL) were collected to measure extracellular LDH. Adherent cells were then lysed with 100 µL of 1% (v/v) Triton X-100 in PBS for 20 min at 37 °C to release intracellular LDH. Equal volumes of reaction mixture were added to both supernatant and lysate samples, and the plates were incubated for 20 min at room temperature in the dark. Absorbance was recorded at 450 nm (14). Background (medium + reagents without cells) and medium controls (drug + medium without cells) were subtracted. The percentage of LDH release was calculated for each condition using the following equation:

$$\text{LDH Release \%} = (A_{Supernatant}/A_{Supernatant}+A_{Lysate})\times100$$

Where $A_{Supernatant}$ and A_{Lysate} represent background-corrected absorbance values of the extracellular and intracellular fractions, respectively. Each condition was assayed in triplicate, and results are presented as mean ± SE.

Annexin V-FITC/PI apoptosis assay

An Annexin V-FITC/PI Apoptosis Detection Kit (Elabscience Bionovation Inc.) was used to assess apoptosis in 4T1 cells. Cells were seeded in 24-well plates at 1×10^5 cells/well and treated with 67 µg/ml RL10 for 72 hr. After treatment, cells were washed with PBS and trypsinized; trypsinization was neutralized with complete medium, and cells were collected by centrifugation (300 × g, 5 min). The pellet was washed once with PBS, resuspended in 500 µl of

1× Annexin V Binding Buffer (one-step protocol), and 5 µl Annexin V-FITC and 5 µl Propidium iodide (PI) were added. Samples were gently mixed and incubated in the dark at room temperature for 15–20 min. Compensation was performed using single-stained controls for Annexin V-FITC and propidium iodide to correct for spectral overlap between fluorescence channels. The binding of these dyes to the apoptotic cells was explored using a flow cytometer (FITC channel for Annexin V; PerCP/Cy5.5 channel preferred for PI). The plot has four quadrants: Q4 (both dyes are negative) shows the number of viable cells. The Q3 (PI is negative and FITC Annexin V is positive) indicates the number of early apoptotic cells. The Q2 (both dyes are positive) demonstrates late apoptotic cells. The Q1 (PI is positive and FITC Annexin V is negative) indicates dead cells, either late-stage apoptosis or necrosis (5).

Caspase 3/7 activity assay

Caspase-3/7 activity in 4T1 cells was quantified using the Kiazist Caspase-3/7 colorimetric assay kit (Catalog number: KCAS37) according to the manufacturer's instructions. After treatment with 67 µg/ml of RL10, cells were lysed in Caspase Lysis Buffer on ice, and the clarified supernatants were collected by centrifugation. Equal volumes of cell lysates were added to each well of a 96-well plate, followed by addition of the reaction mixture containing Caspase Buffer, Dithiothreitol (DTT), and the chromogenic substrate Asp–Glu–Val–Asp-*p*-nitroaniline (DEVD-*p*NA). After incubation at 37 °C for 2 hr, the absorbance was measured at 405 nm using a microplate reader (15). A *p*NA standard curve was used to calculate enzyme activity, which was expressed as milliunits per milliliter (mU/ml) of lysate. All experiments were performed in triplicate under identical conditions, and results are presented as mean ± SE.

Cell cycle distribution assay

4T1 cell cycle states were investigated by PI staining. Cells were cultured and rinsed in PBS. To fix the cells, 1 ml of cold 70% ethanol was added gradually to the cell pellet. After centrifugation at 500 x g for 5 min, the resuspended cells were washed twice with buffer. To eliminate RNAs, 50µl of RNase A solution (Yektatajhuziz, Iran, Cat. No.: YT9055) was directly added to the pellet. 400µl PI solution (Sigma-Aldrich, CAS No.: 25535-16-4) per million cells was added to the solution, mixed well, and incubated in the dark at 37 degrees for 20 min. Debris was excluded by gating on forward and side scatter parameters. Doublets were eliminated using FL2-A versus FL2-W pulse geometry plots. The DNA content histogram was generated based on PI fluorescence (FL2-A), and the percentages of cells in the G0/G1, S, and G2/M phases were identified using a BD FACSCalibur flow cytometer and Flow Jo software (5).

Molecular analysis

RNA extraction

Incubation of 4T1 cells with 67 µg/ml of the peptide and untreated cells as a negative control was performed for 48 hr. Cells were washed with phosphate buffer saline, and total RNA extraction was carried out using Trizol reagent (ELK Biotechnology, USA), according to the manufacturer's instructions. All experiments were conducted under conditions that prevent RNase contamination, and were performed in triplicate. The integrity of the RNA was assessed through agarose gel electrophoresis by examining the 18S and 28S ribosomal RNA bands. The concentration and quality of the RNA were determined by measuring the optical density at 260/280 nm using a NanoDrop spectrophotometer (5).

cDNA synthesis

A cDNA synthesis kit from Sinaclon, BioScience, along with reverse transcription PCR (RT-PCR), was employed to convert RNA into complementary DNA (cDNA), following the instructions provided by the manufacturer.

Real-time PCR

The expression levels of the *Bax*, *Bcl2*, *Casp8*, *Casp9*, and *p53* genes were analyzed through qPCR and the Master Mix (Toyobo, Japan) using primers whose sequences are listed in (5). The PCR cycling conditions were set as follows: initial denaturation at 95 °C for 15 min, followed by 40 cycles of denaturation at 95 °C for 15 sec, annealing at 60 °C for 30 sec, and extension at 72 °C for 30 sec. Following amplification, melt curve analysis was performed to verify the specificity of the PCR products. The melt curve was generated by gradually increasing the temperature from 60 °C to 95 °C, and the presence of a single peak confirmed specific amplification without nonspecific products or primer-dimer formation. All experiments were carried out using three separate cDNA preparations. The data were normalized against the housekeeping gene, *GAPDH*. The results were analyzed using the Relative Expression Software Tool (REST, QIAGEN) and the $2^{-\Delta Ct}$ formula.

In vivo studies

Animals and ethics statements

All protocols concerning the treatment of laboratory mice received approval from the relevant guidelines of the Ethical Committee at Yazd University (Approval ID: IR.YAZD.REC.1404.012). Six to eight-week-old inbred female BALB/c mice were obtained from the Institute Pasteur of Iran and maintained on a consistent light and dark cycle, with food and water available without restriction (ad libitum). Humane endpoint criteria included excessive tumor growth, ulceration at the tumor site, significant body weight loss, or signs of severe distress.

Tumor growth assessment in mice

To induce a tumor, 5×10^5 4T1 cells were injected subcutaneously into the right flank of the mice. When the tumor volume reached 150 mm^3, five mice were randomly allocated to each group. The treatment and control groups received an intraperitoneal injection of 5 mg/kg/day of the peptide or an equivalent volume of PBS, respectively, for 2 weeks. Mice were monitored closely for any abnormal signs, and their body weights were recorded every other day. Tumor diameters were measured every other day using a caliper. Tumor volume was calculated using the formula ((shortest diameter)^2 × longest diameter × 0.52) (13)Canstatin, and Tumstatin, respectively. The research identified that the two overlapping peptides derived from Tumstatin are more effective than other fragments and amino acids L78, V82, and D84 are essential for their activity. In the present study, the efficacy of a nine amino acid peptide derived from Tumstatin (Tum). Data are presented as average ± standard error. Ultimately, the mice were anesthetized by injection

of the anesthetics Ketamin (100 mg/kg) and Xylazine (10 mg/kg) in a ratio of 10:1, then euthanized using the cervical vertebrate displacement method. The tumors were excised and processed for histological analysis.

H&E staining and histopathology

After euthanasia, tumor samples were preserved in 10% formalin, dehydrated using a series of alcohol solutions, embedded within paraffin, and then sectioned. Subsequently, the 3- to 5-µm sections were sliced from the paraffin blocks, placed onto slides, and allowed to air dry. The slides underwent deparaffinization in xylene, rehydration in a graded ethanol series, staining with Hematoxylin and Eosin (H & E), and rinsing with water. The tissue sections were examined under light microscopy, and the numbers of mitotic cells, apoptotic cells, Tumor-Infiltrating Lymphocytes (TILs), and tumor necrosis were documented in 10 High Power Fields. Additionally, the degree of nuclear pleomorphism (differences in size and shape) was assessed using a scoring system from 1 to 3, with 3 indicating the highest level of abnormality (16). Scoring was performed by a blinded pathologist. Averages were computed for both the control and treatment groups, and the data were presented as mean ± SE. The slides were captured using a digital camera at 100x magnification.

Statistical analysis

The data were processed using SPSS version 22. A Student's t-test was used to compare the means of two groups. Results are presented as average ± standard error, with a significance threshold of $P< 0.01$.

Results

Cell viability assessment using MTT

Cytotoxicity of the peptide at different concentrations against 4T1 and SW480 cell lines was assessed by MTT assay at 48 hr and 72 hr (n=3). As demonstrated in Figure 1A and 1B, the peptide decreased the viability of both cell lines in a dose-dependent manner ($P<0.01$). The effect in SW480 was in a time-dependent manner ($P<0.01$) (Figure 1A), but in 4T1 it peaked at 48 hr and decreased at 72 hr ($P<0.01$) (Figure 1B). For the 4T1 cells, the half-maximal inhibitory concentration (IC_{50}) values were 67.03 µg/ml at 48 hr and 187.9 µg/ml at 72 hr ($P<0.01$). In SW480 cells, the IC_{50} values were 146.9 µg/ml at 48 hr and 83.35 µg/ml at 72 hr ($P<0.01$). According to these results, 67 µg/ml and 48 hr' incubation time were used for other *in vitro* assessments on 4T1. Furthermore, the peptide's effect on NIH3T3 cells, a normal cell line, was identified (Figure 1C). The IC_{50} values were 208.5 µg/ml at 48 hr ($P<0.01$).

Cytotoxicity assessment using LDH release

The cytotoxic effect of the peptide (67 µg/ml) on the 4T1 cell line was further evaluated using the lactate dehydrogenase (LDH) assay (n=3). In this assay, when the cell membrane is damaged or the cell dies, LDH is released into the extracellular space, and the amount of LDH correlates with the number of dead or injured cells. As illustrated in Figure 1D, LDH released in the cells treated by the peptide was less than that of the negative control ($P<0.01$).

Apoptosis and cell cycle arrest evaluation by flow cytometry

The peptide induced 28.9% apoptosis, comprising 14.7% early apoptosis and 14.2% late apoptosis, in the 4T1 cells, which was statistically significant compared with the control (n=3) ($P<0.01$) (Figure 2A to 2C). Cell cycle analysis demonstrated that the peptide induced 8.1% and 8.7% increase in S and G2/M phases, respectively ($P<0.01$), and 17.2% reduction in G0/G1 phase, compared with the control ($P<0.01$) (Figure 2D to 2F).

Evaluation of caspase 3/7 activity

Caspase 3/7 activity was measured to examine apoptosis induction in 4T1 cells after treatment with 67 µg/ml of RL10 (n=3) (Figure 3A). The measured caspase-3/7 activity values were 4.143 mU/ml in the treated group and 2.506 mU/ml

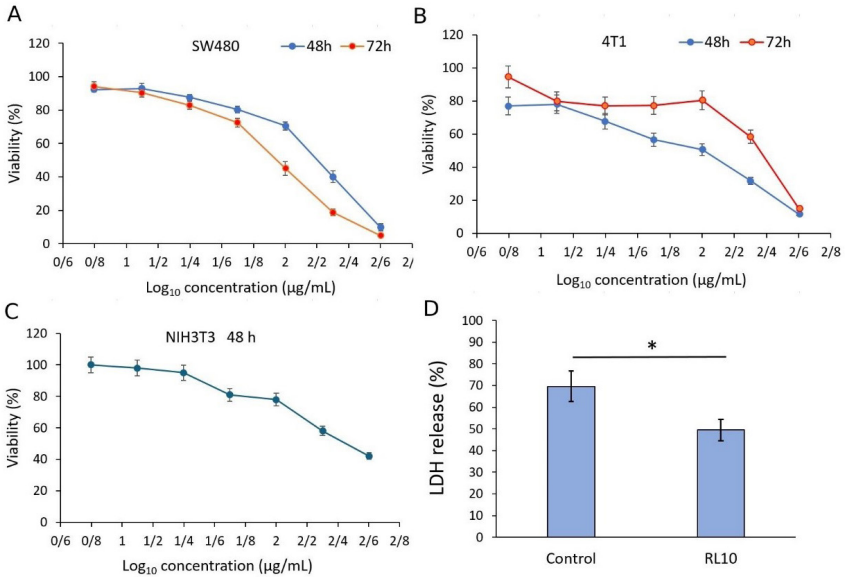

Figure 1. Cell viability and cytotoxicity effects of RL10 peptide on different cell lines

A) Percentage of viable SW480 cells, B) 4T1 cells, and C) NIH3T3 cells, as determined by the MTT assay after 48 and 72 hr of incubation with various concentrations of RL10. D) Lactate dehydrogenase (LDH) release in 4T1 cells following treatment with 67 µg/ml RL10 for 48 hr. Data are expressed as mean ± SE of three independent experiments. *$P<0.01$ vs control, indicating a statistically significant difference.

MTT: 3-(4,5-dimethylthiazol-2-yl)-2,5-diphenyltetrazolium bromide; RL10: Arginine-rich decapeptide

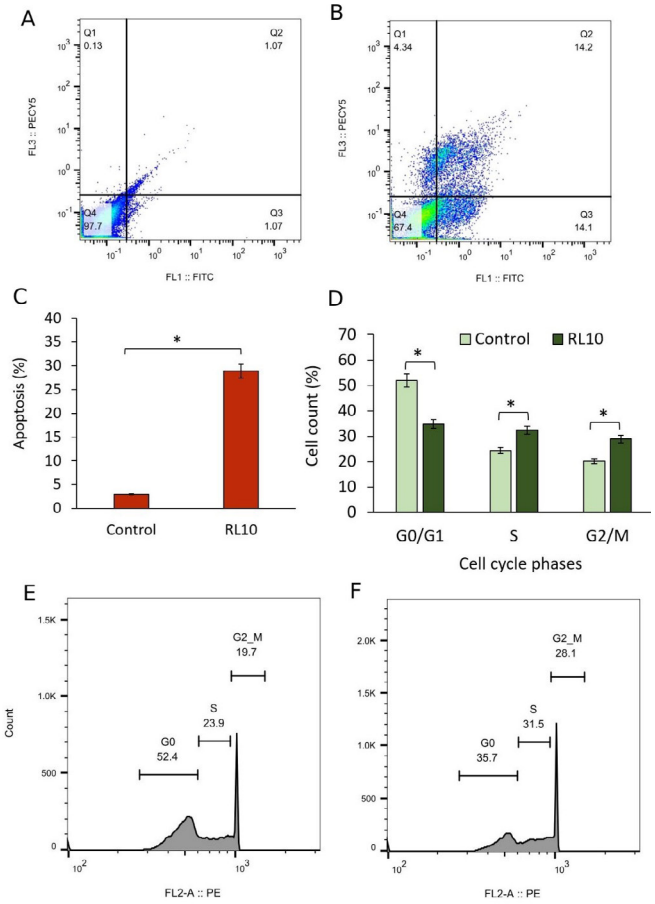

Figure 2. Flow cytometry analysis of apoptosis and cell cycle distribution in 4T1 cells treated with the RL10 peptide

A) Apoptosis in untreated control cells and B) cells treated with 67 µg/ml RL10 for 48 hr were analyzed by flow cytometry. C) Quantitative representation of total apoptotic cells (sum of early and late apoptosis). D–F) Cell cycle distribution analysis of 4T1 cells: D) representative plot, E) control group, and F) RL10-treated group. Data are presented as mean ± SE from three independent experiments. *P<0.01 vs control, indicating a statistically significant difference.
RL10: Arginine-rich decapeptide

in the negative control group (Figure 3A). Accordingly, the caspase-3/7 activity in RL10-treated cells was approximately 1.65-fold higher than that observed in the control group (P<0.01).

Evaluation of apoptosis gene expression using RT-PCR

Expression of *Bax*, *Bcl2*, *p53*, *Casp8*, and *Casp9* genes was measured to further evaluate apoptosis in the 4T1 cell line (n=3). As demonstrated in Figure 3B, Caspase9 gene (*Casp9*) was significantly up-regulated in the cells treated with the peptide (P<0.01), while other gene expressions did not significantly affect by the peptide (P>0.01).

Evaluation of tumor growth in vivo

5 mg/kg/day of the peptide was injected into the 4T1 tumor-bearing mice (n=5) for two weeks, and the tumor volume was calculated (Figure 4A and 4B). At the end of treatment, average tumor volume reached 1651 and 1010 mm^3 in the control and treatment groups, respectively, and the peptide inhibited tumor growth by 38.8% compared with the control group (P<0.01) (Figure 4A and 4B). The mice's body weight on the first day of treatment in the

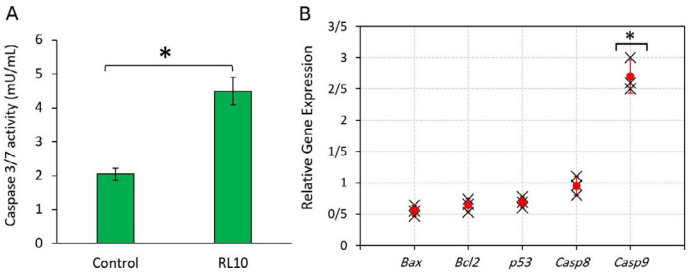

Figure 3. Evaluation of apoptosis-related markers in 4T1 cells following treatment with the RL10 peptide

A) Caspase-3/7 enzymatic activity and B) relative gene expression levels analyzed by RT-PCR after treatment with 67 µg/ml RL10 for 48 hr. In panel B, each cross represents an individual replicate, and the red dot indicates the mean of the replicates. Data are presented as mean ± SE from three independent experiments. *P<0.01 vs control, indicating a statistically significant difference. RL10: Arginine-rich decapeptide

control and treatment groups was 21.24 and 22.81 grams, respectively, and at the end of the study was 20.96 and 27.81, respectively. No observable toxicity or adverse effects were noted in treated mice.

Histopathological evaluation of tumors

Histopathological features of the tumors were evaluated by H&E staining. Scoring was performed by a blinded pathologist according to the predefined criteria (Figure 4C and 4D). The results showed that tumor necrosis and nuclear pleomorphism (variation in shape and size) did not significantly change in the treated compared with the control group (P>0.01), while apoptotic figures count and Tumor-Infiltrating Lymphocytes (TILS) increased and mitotic count decreased significantly compared with the control (Table 1) (P<0.01).

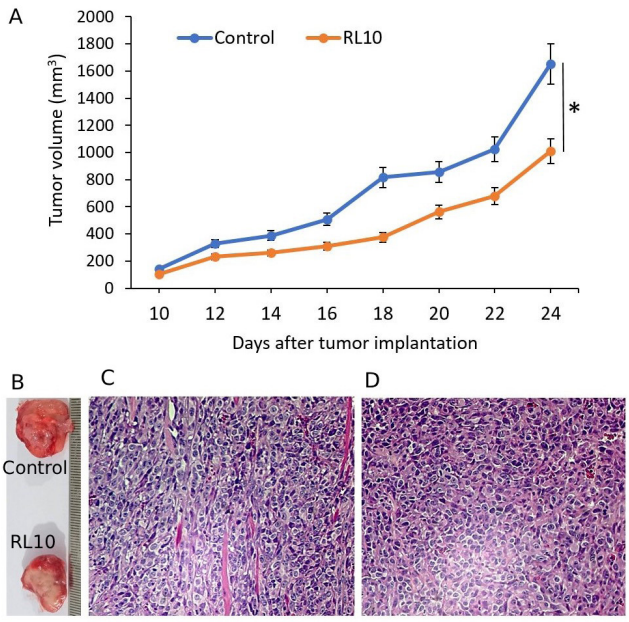

Figure 4. Antitumor efficacy of the RL10 peptide in 4T1 tumor-bearing mice

A) Tumor volume in mice treated with 5 mg/kg/day RL10 via IP injection. Data are presented as mean ± SE (n = 5 mice per group). *P<0.01 vs control, indicating a statistically significant difference. B) Excised tumors collected at the end of the study. C–D) Histopathological analysis (H&E staining) of tumor tissues: C) control group and D) RL10-treated group.
RL10: Arginine-rich decapeptide; IP: Intraperitoneal

Table 1. Histopathological features of the tumors

	Tumor necrosis	Nuclear pleomorphism	Apoptotic figures count	TILS	Mitotic count
Control	60-70%±2.87	+3±0.98	5±1.08	less than 1%±0.76	40±3.02
RL10	60-70%±2.45	+3±1.02	10±1.56 [a]	less than 3%±0.84[b]	30±2.63 [c]

a, b, and c show statistically significant differences between the treatment and the related control group (P<0.01).
RL10: Arginine-rich decapeptide; TILS: Tumor-Infiltrating Lymphocytes

Discussion

The present study evaluated the anticancer activity of a short cationic peptide, RL10, enriched in arginine residues, *in vitro* and *in vivo*. The findings suggest that this peptide exerts selective cytotoxic and pro-apoptotic effects in 4T1 cells and demonstrates measurable antitumor activity in tumor-bearing mice.

A 12-amino acid cathelicidin-derived antimicrobial peptide, named 1018-K6, and its shorter derivative, named RiLK1, were developed in silico, and their antibacterial features were characterized deeply (17). In another study, a RiLK1 derivative with a single lysine-to-arginine substitution was created and named RiLK3 (12). The peptide was characterized as a broad-spectrum antibacterial agent that selectively interacts with negatively charged membranes. Structural studies revealed that the peptide adopts a mixture of α-helix, β-sheet, and random coil conformation in membrane-mimicking environments (12). Despite its well-documented antimicrobial properties, the peptide's anticancer potential had not been investigated until the present study. Here, RiLK3 was renamed to RL10.

The present study revealed that this peptide reduced the viability of both 4T1 and SW480 cells in a dose-dependent manner, although the temporal pattern differed between the two cell lines. The more pronounced reduction in viability at 48 hr in 4T1 cells followed by a partial recovery at 72 hr may reflect adaptive cellular responses or reduced peptide stability in culture conditions. In contrast, the enhanced effect at 72 hr in SW480 cells indicates a delayed but progressive cytotoxic action, hypothesizing differences in cellular uptake or susceptibility between epithelial and mammary tumor cells. Such non-linear or non–time-dependent patterns in MTT results have been described before, since the assay measures mitochondrial metabolic activity rather than direct cell number, and factors such as metabolic adaptation or formazan accumulation may confound time-dependent trends (18). These differences highlight the importance of tumor-specific context when evaluating novel peptides.

Currently, only a limited number of active peptides of 10 residues, such as RL10, have been reported. In general, most cationic antimicrobial peptides with anticancer properties are longer than 10 amino acids. For example, one study showed that cationic peptides of 6 (LFcinB6) and 11 (LFcinB11) amino acids derived from lactoferricin, despite containing the antimicrobial core RRWQWR, exhibited no cytotoxic effect against cancer cells (IC_{50} > 500 μM). Their limited activity was attributed to weak mitochondrial binding and the inability to trigger apoptosis. In contrast, the 25-amino acid fragment LFcinB25 showed potent anticancer activity against AGS cells (IC_{50} ≈ 64 μM), inducing both apoptosis and autophagy (19). I-7, a 15-mer arginine-rich peptide derived from host defense peptide B1, showed strong cytotoxicity against MCF-7, K562, and HeLa cells after 48 hr, with the IC_{50} values ranging from 4.2 to 6.9 μM (15). The 25-mer cationic spider venom–derived peptide LyeTx I-b showed cytotoxicity against the 4T1 cell line after 48 hr, with an IC_{50} of 6.5 μM (20). RT2, 17-mer arginine- and tryptophan-modified derivatives of Leucrocin I, exhibited notable cytotoxicity against HeLa cells after 24 hr, with the IC_{50} values of 28.6 μM (21). Mastoparan, a 14-residue cationic peptide from wasp venom, displayed anticancer activity against 4T1 cells after 24 hr (IC50: 20–24 μM) (22). Although the IC_{50} of RL10 (67 μg/ml ≈ 44.8 μM) is higher than the mentioned peptides, the shorter length of this peptide highlights the novelty and importance of our findings, as it suggests that short arginine-rich peptides can also achieve potent anticancer effects.

There are conflicting reports regarding the cytotoxicity of arginine-rich peptides. While some studies have shown that these peptides are more toxic to normal cells (23, 24), other studies have reported little or no toxicity toward normal cells (15, 21, 25). In the present study, IC_{50} values of RL10 in normal cells were much higher than those in cancer cells, indicating that the peptide does not have a toxic effect on normal cells.

Interestingly, the peptide did not increase LDH release in 4T1 cells; in fact, LDH levels were lower than in untreated controls. In cytotoxicity assays, higher LDH levels in the medium signify cell death and membrane damage. A lower LDH concentration in the treatment group's medium compared with the control indicates that the cells are more intact and less damaged. This finding suggests that the treatment either protects cells from a toxic insult, promotes cell survival, or reduces cellular necrosis. This result indicates that the peptide's cytotoxic action is unlikely to occur through necrotic membrane damage. The apparent discrepancy with the MTT results could raise questions. This might be explained by the fact that MTT reduction is a metabolic measure and may decline before overt membrane damage is detectable. The MTT assay cannot differentiate between apoptosis and necrosis. In comparison, the LDH release assay offers information on cell membrane integrity and is more indicative of necrotic cell death (26). Our results contrast with those of others, who showed that treating cancer cells with cationic peptides increased lactate dehydrogenase release (14, 15, 25).

Annexin V-FITC/PI staining confirmed a marked induction of apoptosis in 4T1 cells, with nearly 29% of cells undergoing apoptosis. Furthermore, the peptide caused accumulation of cells in the S and G2/M phases, coupled with depletion of the G0/G1 population. Cell cycle arrest and apoptosis are closely interconnected processes regulated by multiple signaling pathways, including tumor suppressor p53 (27), CDK inhibitors (p21, p27) (28), JNK and p38 MAPK (29), PI3K/AKT/mTOR (30), and TGF-β signaling (31). The combined effects of the peptide on apoptosis and the cell cycle support a mechanism involving cell cycle

arrest–mediated apoptosis. However, further mechanistic assays, such as detection of mitochondrial membrane potential or reactive oxygen species, are needed to confirm the involvement of mitochondrial pathways.

Our results are in line with Nguyen *et al.*, who demonstrated that 2.5 to 10 μM of a 24-mer cationic antimicrobial peptide Smp24, originating from scorpion venom, induces apoptosis (by 38%) and G2/M cell cycle arrest in HepG2 cells after 24 hr (25). In addition, Dong *et al.* reported that a 34-mer cationic antibacterial peptide markedly induced apoptosis in SGC-7901 and HepG-2 cells. The peptide also triggered G0/G1 cell cycle arrest (32).

To better examine apoptosis in 4T1 cells, caspase-3/7 activity was assessed. Accordingly, the peptide significantly increased caspase 3/7 activity compared to the control. The observed increase in caspase-3/7 activity in the treated group confirms the peptide's pro-apoptotic effect. Caspases-3 and -7 act as key executioner enzymes in the final stages of apoptosis, leading to cleavage of vital cellular substrates and cell death (33). Therefore, their activation indicates that the peptide induces apoptosis through activation of the execution phase of the apoptotic pathway. This result is in line with previous studies showing that cationic peptides triggered caspase-3 activity (15, 32, 34).

The expression of different genes involved in apoptosis was also measured. Only *CASP9* was significantly upregulated, while *Bax*, *Bcl-2*, *p53*, and *CASP8* remained unchanged. Since caspase-9 is a key enzyme in the intrinsic apoptotic pathway (33), these findings suggest a possible involvement of the mitochondrial pathway. However, a more detailed understanding of this peptide's apoptotic mechanism is recommended through additional experiments, such as assessing mitochondrial disruption, cytochrome c release, and protein levels by Western blot. It should also be noted that, despite limited transcriptional changes, previous research has reported that apoptosis induced by cationic peptides is often associated with alterations in Bax and Bcl2 protein expression (32, 34) and/or caspase-9 activity (32, 34).

Daily administration of RL10 (5 mg/kg/day) reduced tumor volume by nearly 39% (P<0.01), demonstrating a tangible antitumor effect in a murine model. Humane endpoint criteria were predefined and applied throughout the study. No criteria were observed. Histology supported the molecular data, showing increased apoptotic figures and tumor-infiltrating lymphocytes, as well as decreased mitotic activity in treated tumors. The unchanged necrosis and nuclear pleomorphism indicate that the peptide's main effect was functional rather than structural tumor disruption. These results are consistent with previous reports on other cationic anticancer peptides. For instance, Abdel-Salam *et al.* showed that intratumoral injection of the LyeTx I-b peptide (5 mg/kg/day, a dose similar to that in the present study) prevented tumor growth by up to 52% in a 4T1 breast cancer model and reduced lung metastasis (20). Similarly, 6 mg/kg of Mastoparan (IP, every two days) significantly suppressed 4T1 tumor growth in mice more than 50% (22), while Nguyen *et al.* demonstrated that injection of Smp24 peptide near the tumor site (2 mg/kg, every three days) inhibited tumor growth up to 56% in a HepG2 xenograft model (25). Differences in peptide sequence, net charge, length, dosing regimen, and treatment duration likely account for the variability in tumor response across these studies.

Conclusion

In summary, our findings suggest that the arginine-rich decapeptide RL10 exerts anticancer effects against both murine breast (4T1) and human colorectal (SW480) cancer cells. The peptide reduces cell viability in a dose-dependent manner, promotes apoptosis, and induces cell cycle arrest in 4T1 cells, and shows no toxicity toward normal cells or *in vivo* models. Its activity appears to be non-lytic, as evidenced by the absence of LDH release. *In vivo*, the peptide significantly suppressed tumor growth without detectable toxicity, accompanied by enhanced apoptotic activity and increased tumor-infiltrating lymphocytes. While the degree of tumor inhibition was moderate and some mechanistic aspects remain to be clarified, the dual nature of RL10, combining antimicrobial efficacy with newly demonstrated anticancer activity, together with the broader applications of arginine-rich peptides in drug delivery, blood–brain barrier penetration, and biosensors, emphasizes on their potential as candidates for repurposing in oncology, either as stand-alone treatments or in combination with conventional therapies. Further studies are warranted to explore RL10's pharmacokinetics, delivery strategies, and combinatorial potential with existing therapies.

Acknowledgment

The authors would like to express their sincere appreciation to Yazd University, Iran, for its support and assistance in conducting this research.

Funding

The authors declare that no funds, grants, or other support while preparing this manuscript.

Authors' Contributions

R Ch designed the study, performed experiments, and collected data; R Ch and M M analyzed the results; M M wrote the first draft of the manuscript and prepared the figures. All authors read and approved the final manuscript.

Conflicts of Interest

The authors disclose no conflicts of interest.

Declaration

The authors declare that Artificial Intelligence (AI)-assisted tools (Grammarly and ChatGPT) were used solely for language editing, grammar checking, and improving the manuscript's readability. All scientific content and writing were generated by the authors, who take full responsibility for the work's integrity and accuracy.

References

1. Wilkinson L. Understanding breast cancer as a global health concern. Br J Radiol 2022; 95: 1-8.
2. Sood A, Jothiswaran V V, Singh A, Sharma A. Anticancer peptides as novel immunomodulatory therapeutic candidates for cancer treatment. Explor Target Anti-tumor Ther 2024; 5: 1074-1099.
3. Bauso LV, La Fauci V, Munaò S, Bonfiglio D, Armeli A, Maimone N, *et al.* Biological activity of natural and synthetic peptides as anticancer agents. Int J Mol Sci 2024; 25: 1-19.
4. Sarabi N, Chamani R, Assareh E, Saberi O, Asghari SM. Combination therapy in cancer: Doxorubicin in combination with an N-terminal peptide of endostatin suppresses angiogenesis and stimulates apoptosis in the breast cancer. Int J Mol Cell Med 2023;

12: 1-15
5. Chamani R, Saberi O, Fathinejad F. An arresten-derived anti-angiogenic peptide triggers apoptotic cell death in endothelial cells. Mol Biol Rep 2024; 51: 1-11
6. Nhàn NTT, Yamada T, Yamada KH. Peptide-based agents for cancer treatment: Current applications and future directions. Int J Mol Sci 2023; 24: 1-15.
7. Meloni BP, Mastaglia FL, Knuckey NW. Cationic arginine-rich peptides (CARPs): A novel class of neuroprotective agents with a multimodal mechanism of action. Front Neurol 2020; 11: 1-20
8. Liscano Y, Oñate-Garzón J, Delgado JP. Peptides with dual antimicrobial–anticancer activity: Strategies to overcome peptide limitations and rational design of anticancer peptides. Molecules 2020; 25: 1-20
9. Bucataru C, Ciobanasu C. Antimicrobial peptides: Opportunities and challenges in overcoming resistance. Microbiol Res 2024; 286: 1-15.
10. Varela-Quitián YF, Mendez-Rivera FE, Bernal-Estévez DA. Cationic antimicrobial peptides: Potential templates for anticancer agents. Front Med 2025; 12: 1-16.
11. Dong Z, Zhang X, Zhang Q, Tangthianchaichana J, Guo M, Du S, *et al.* Anticancer mechanisms and potential anticancer applications of antimicrobial peptides and their nano agents. Int J Nanomedicine 2024; 19: 1017-1039.
12. Agrillo B, Porritiello A, Gratino L, Balestrieri M, Proroga YT, Mancusi A, *et al.* Antimicrobial activity, membrane interaction and structural features of short arginine-rich antimicrobial peptides. Front Microbiol 2023; 14: 1-20.
13. Chamani R, Taleqani MH, Imanpour A, and Khatami M. New insights into short peptides derived from the collagen NC1 α1, α2, and α3 (IV) domains: An experimental and MD simulations study. Biochim Biophys Acta - Proteins Proteomics 2022; 1870: 1-10.
14. Hu C, Chen X, Huang Y, Chen Y. Synergistic effect of the pro-apoptosis peptide kla-TAT and the cationic anticancer peptide HPRP-A1. Apoptosis 2018; 23: 132-142.
15. Dai Y, Cai X, Shi W, Bi X, Su X, Pan M, *et al.* Pro-apoptotic cationic host defense peptides rich in lysine or arginine to reverse drug resistance by disrupting tumor cell membrane. Amino Acids 2017; 49: 1601-1610.
16. Chamani R, Darvand-Araghi MH. Disulfide bond : A critical element in the structure and function of a collagen IV-derived antiangiogenic peptide. 2025; 5: 289-303.
17. Agrillo B, Proroga Y, Gogliettino M, Balestrieri M, Tate R, Nicolais L, *et al.* A safe and multitasking antimicrobial decapeptide: The road from de novo design to structural and functional characterization. Int J Mol Sci 2020; 21: 1-22.
18. Van Tonder A, Joubert AM, Cromarty AD. Limitations of the 3-(4, 5-dimethylthiazol-2-yl)-2, 5-diphenyl-2H-tetrazolium bromide (MTT) assay when compared to three commonly used cell enumeration assays. BMC Res Notes 2015; 8: 1-10.
19. Pan W R, Chen P W, Chen Y L, Hsu H C, Lin C C, Chen W J. Bovine lactoferricin B induces apoptosis of human gastric cancer cell line AGS by inhibition of autophagy at a late stage. J Dairy Sci 2013; 96: 7511-7520.
20. Abdel-Salam M, Pinto B, Cassali G, Bueno L, Pêgas G, Oliveira F, *et al.* LyeTx Ib peptide attenuates tumor burden and metastasis in a mouse 4T1 breast cancer model. Antibiotics 2021; 10: 1-28.
21. Theansungnoen T, Maijaroen S, Jangpromma N, Yaraksa N, Daduang S, Temsiripong T, *et al.* Cationic antimicrobial peptides derived from Crocodylus siamensis leukocyte extract, revealing anticancer activity and apoptotic induction on human cervical cancer cells. Protein J 2016; 35: 202-211.
22. Hilchie AL, Sharon AJ, Haney EF, Hoskin DW, Bally MB, Franco OL, *et al.* Mastoparan is a membranolytic anti-cancer peptide that works synergistically with gemcitabine in a mouse model of mammary carcinoma. Biochim Biophys Acta (BBA)-Biomembranes 2016; 1858: 3195-3204.
23. Hadianamrei R, Tomeh MA, Brown S, Wang J, Zhao X. Rationally designed short cationic α-helical peptides with selective anticancer activity. J Colloid Interface Sci 2022; 607: 488-501.
24. Arias M, Haney EF, Hilchie AL, Corcoran JA, Hyndman ME, Hancock REW, *et al.* Selective anticancer activity of synthetic peptides derived from the host defence peptide tritrpticin. Biochim Biophys Acta (BBA)-Biomembranes 2020; 1862: 1-10.
25. Nguyen T, Guo R, Chai J, Wu J, Liu J, Chen X, *et al.* Smp24, a scorpion-venom peptide, exhibits potent antitumor effects against hepatoma HepG2 cells via multi-mechanisms *in vivo* and *in vitro*. Toxins (Basel) 2022; 14: 1-19.
26. Singhal M, Shaha S, Katsikogianni M. Comparative analysis of cytotoxicity assays, from traditional to modern approaches. From edited volume: Cytotoxicity-a crucial toxicity test for *in vitro* experiments (Edited by: Erkekoglu P.). IntechOpen 2025. p. 1-54
27. Wang H, Guo M, Wei H, Chen Y. Targeting p53 pathways: Mechanisms, structures, and advances in therapy. Signal Transduct Target Ther 2023; 8: 1-35.
28. D'costa M, Bothe A, Das S, Kumar SU, Gnanasambandan R, Doss CGP. CDK regulators: Cell cycle progression or apoptosis-Scenarios in normal cells and cancerous cells. Adv Protein Chem Struct Biol 2023; 135: 125-177.
29. Yue J, López JM. Understanding MAPK signaling pathways in apoptosis. Int J Mol Sci 2020; 21: 1-22.
30. Pungsrinont T, Kallenbach J, Baniahmad A. Role of PI3K-AKT-mTOR pathway as a pro-survival signaling and resistance-mediating mechanism to therapy of prostate cancer. Int J Mol Sci 2021; 22: 1-25.
31. Yu Y, Feng X-H. TGF-β signaling in cell fate control and cancer. Curr Opin Cell Biol 2019; 61: 56-63.
32. Dong L, Li Y, Zhang Y, Su S. Cationic antimicrobial peptide CC34 potential anticancer and apoptotic induction on cancer cells. Amino Acids 2025; 57: 1-13.
33. Mustafa M, Ahmad R, Tantry IQ, Ahmad W, Siddiqui S, Alam M, *et al.* Apoptosis: A comprehensive overview of signaling pathways, morphological changes, and physiological significance and therapeutic implications. Cells 2024; 13: 1-20.
34. Liu S, Aweya JJ, Zheng L, Zheng Z, Huang H, Wang F, *et al.* LvHemB1, a novel cationic antimicrobial peptide derived from the hemocyanin of Litopenaeus vannamei, induces cancer cell death by targeting mitochondrial voltage-dependent anion channel 1. Cell Biol Toxicol 2022; 38: 87-110.